Preparation and structural investigation of epitaxially grown antiferromagnetic FeSn2(001) thin films on InSb(001)

doi: 10.1063/1.1595144

Preparation and structural investigation of epitaxially grown antiferromagnetic $FeSn_2(001)$ thin films on InSb(001)

V. Kuncser,[a] M. Doi,[b] B. Sahoo, F. Stromberg, and W. Keune[c]
Laboratorium für Angewandte Physik, Gerhard-Mercator-Universität, Lotharstrasse 65, D-47048 Duisburg, Germany

(Received 18 December 2002; accepted 4 June 2003)

Antiferromagnetic $FeSn_2(001)$ thin films with different thicknesses and relatively low Néel temperatures were grown on InSb(001)(4×2) surfaces by molecular-beam epitaxy. The Néel temperature could be increased to above room temperature by subsequent thermal annealing. *In situ* structural characterization was performed by high- and low-energy electron diffraction. The degree of the structural (001) texture as a function of the preparation and annealing conditions was investigated by x-ray diffractometry. The local magnetic properties and the spin structure were studied using ^{57}Fe conversion electron Mössbauer spectroscopy (CEMS) at different temperatures. The epitaxial $FeSn_2(001)$ thin films exhibit in-plane Fe spin orientation and appear to be suitable antiferromagnets for studying the interfacial spin structure in exchange-biased bilayers by CEMS.
 [DOI: 10.1063/1.1595144]

I. INTRODUCTION

Pinning effects at the interface of magnetic bilayer systems with different magnetic anisotropies lead to interesting physical phenomena. Between them, the exchange-bias effect has found important applications, especially in spin-valve devices.[1–4] This phenomenon is related to the unidirectional anisotropy induced at the interface between a soft ferromagnetic (FM) and an antiferromagnetic (AF) material with high magnetic anisotropy, when the system is prepared in a magnetic field or cooled in an applied magnetic field through the Néel temperature T_N of the AF phase. Although the effect was discovered in 1956,[5] its microscopic origin has not yet been fully understood. The available theoretical models differ substantially depending on the assumed interfacial spin structure.[6–10] Therefore, the knowledge of the real spin structure at the FM/AF interface becomes a very important issue for understanding the microscopic mechanism of the exchange-bias effect.

Mössbauer spectroscopy is a powerful method for studying the spin structure at the interface on an atomic scale in connection with the local crystallographic structure and symmetry. In iron containing thin films, this information can be obtained with high depth selectivity by using ^{57}Fe conversion electron Mössbauer spectroscopy (CEMS), combined with the tracer layer technique, which is based on isotopically enriched ^{57}Fe probe layers (resolution limit of a few atomic layers) artificially placed at the interface or at different depths in a film.[11–14] The only limitation for a suitable study of the Fe spin structure is that the analyzed system should contain Fe atoms with reasonably large magnetic moments, giving rise to high enough magnitudes of the magnetic hyperfine fields in order to resolve properly the nuclear Zeeman sextet and the line intensity ratios in the Mössbauer spectra. Moreover, in order to promote theoretical simulations, the interfacial spin structure should be obtained on structurally simple systems, preferentially on epitaxially grown thin films. Due to the shape anisotropy, the spins of the FM layer are expected to lie in the film plane and, therefore, it is the interfacial spin structure of the AF thin film that is of crucial importance for calculating the exchange bias phenomena in real systems.

The intermetallic compound $FeSn_2$ is an AF material with a Néel temperature of about 378 K in the bulk. Extensive Mössbauer studies have been carried out on this compound,[15–18] because it contains two Mössbauer isotopes (^{57}Fe and ^{119}Sn) and is suitable for studying the transferred hyperfine fields at the Sn atoms. Accordingly, the ^{57}Fe hyperfine magnetic field B_{hf} is known to be about 15 T at 80 K and 11 T at room temperature. The antiferromagnetic $FeSn_2$ phase shows a tetragonal structure[18] (D_{4h}, space group $I4/mcm$, $a=0.653$ nm and $c=0.532$ nm), and its a parameter matches well with the lattice parameter of the cubic InSb crystal (T_d^2, space group $F43m$, $a=0.647$ nm). Results on the magnetic structure in ''pseudo-single-crystals'' of $FeSn_2$ obtained by neutron diffraction, magnetometry, and Mössbauer spectroscopy have been reported by Venturini *et al.*[18] They found that a second magnetic transition occurs at a temperature T_t of about 93 K. Between T_N and T_t, the AF spin structure is collinear, with the Fe spin direction in the (001) plane along the a axis, that is, along [100] directions. Below T_t, the spin structure becomes noncollinear antiferromagnetic, with the Fe magnetic moments forming a canted structure (20° aperture) along the [110] directions. Due to the well-resolved Mössbauer sextet, the convenient Néel temperature, and its interesting magnetic properties, $FeSn_2$ was chosen by us as a proper AF film for the purpose of studying the interfacial spin structure in exchange-biased bilayer systems.

[a]Permanent address: National Institute for Physics of Materials, P.O. Box MG 7, 76900 Bucharest-Magurele, Romania.
[b]Permanent address: Department of Materials Science and Engineering, Nagoya University, Nagoya, Japan.
[c]Author to whom correspondence should be addressed; electronic mail: keune@uni-duisburg.de

In this respect, the present work concentrates on details of the preparation conditions and the complex structural and local magnetic properties of epitaxial thin films of $FeSn_2(001)$ on InSb(001). There are many growth parameters influencing the structural and magnetic properties of $FeSn_2$ thin films, for example, the state of the substrate surface, the growth and annealing temperature, the annealing time, and the film thickness. We present an extensive investigation of various samples prepared under different conditions in order to establish the optimum preparation conditions for epitaxial AF $FeSn_2$ films with T_N values tuned to be appropriate for exchange-bias phenomena. Results on the exchange-bias system $Fe/FeSn_2(001)$ will be reported elsewhere.[19]

II. EXPERIMENTAL PROCEDURE

AF $FeSn_2(001)$ thin films have been grown on commercial InSb(001) wafers by molecular-beam epitaxy (MBE). The substrates were rinsed in acetone and subsequently in ethanol, just before loading into the UHV chamber. Subsequently, they were cleaned by sputtering with low-energy Ar ions (ion energy, current density, and argon partial pressure of 500 eV, 1 $\mu A/cm^2$, and 5.5×10^{-5} mbar, respectively) for 90 min at a temperature of 200 °C followed by annealing for 10–12 h at 350 °C. After this treatment, no surface impurities were detected by Auger electron spectroscopy. Low-energy electron diffraction (LEED) as well as reflection high-energy electron diffraction (RHEED) images of the clean substrate proved that the surface was flat and well ordered, with a (4×2) reconstruction (see subsequent discussion).

The $FeSn_2$ thin films were deposited by co-evaporation of high-purity Fe (99.9985 at. %) and Sn (99.995 at. %) from two independently controlled Knudsen cells at a pressure of 8×10^{-10} mbar during deposition (base pressure of 3×10^{-10} mbar), with a deposition rate of 0.180 nm/min for Fe and 0.822 nm/min for Sn. The evaporation rates were monitored with calibrated quartz-crystal microbalances. These rates determined the nominal composition of the $FeSn_2$ samples. Different substrate temperatures T_s during growth in the range between 25 and 350 °C were used. Tracer layers of $^{57}FeSn_2$ (95% enriched in ^{57}Fe) 5- to 15-nm-thick were deposited onto the surface of the $FeSn_2$ layers of natural isotopic composition (~2% for ^{57}Fe) in order to analyze the interfacial phase composition and spin structure by *ex situ* ^{57}Fe CEMS. The $^{57}FeSn_2/FeSn_2$ structures with total thicknesses t between 15 and 100 nm were finally covered with a 5-nm-thick Sn cap layer for protection. Table I gives the code, film-growth temperature, and total $^{57}FeSn_2/FeSn_2$ film thickness of the different samples.

TABLE I. Sample code, growth temperature T_s and total $^{57}FeSn_2/FeSn_2$ film thickness t of samples.

Sample	T_s (°C)	Thickness t (nm)
A	250	max. 2.7
B	250	max. 2.75
C	200	100
D	250	30
E/(polycr.)	25	15
F	250	30
G	250	15
H	150	20
I	300	15

The surface structure of all $FeSn_2$ thin films has been controlled during growth by RHEED with the electron beam (10 keV; 20 μA) incident at about 3° relative to the sample plane and along the [110] azimuthal direction of the InSb(001) substrate. For samples A and B, the RHEED patterns appearing on the phosphor screen were recorded every few seconds in real time during the growth process by a CCD camera connected to a computer for data storage and image processing. Independent images were also taken in the later stages of growth.

Subsequent *in situ* annealing treatments at temperatures ranging from 250 to 350 °C were performed in UHV on the as-grown films (samples C, D, E, and F) for different annealing times. The film structure after annealing was monitored by LEED and RHEED. LEED images on both as-grown and annealed films could only be obtained at 150 K, because of the low Debye–Waller factor of $FeSn_2$ at RT.

^{57}Fe Mössbauer (CEMS) spectra were measured at RT using a He/CH_4-filled proportional counter. Low-temperature CEMS spectra were recorded by using a channeltron detector that was mounted together with the sample in the evacuated central tube of a liquid-He bath cryostat. A ^{57}Co-in-Rh source was used. The incident γ-radiation was perpendicular to the sample surface. For the least-squares fitting of the CEMS spectra, the NORMOS computer program by Brand[20] was used.

III. RESULTS AND DISCUSSION

A. Films in the as-grown state

1. Structural investigations

The RHEED pattern of a clean InSb(001) substrate taken along the [110] azimuth shows, in addition to the fundamental reflections, the typical streaks of the fourfold surface reconstruction (Fig. 1, top). The (4×2) surface reconstruction of the substrate was also directly confirmed by LEED (not shown). Typical RHEED images of $FeSn_2$ thin films of different thicknesses and grown on InSb(001) at about 250 °C are presented in Fig. 1, left-hand side. The corresponding intensity profiles measured along the horizontal (transverse) direction in k-space are shown in Fig. 1, right-hand side. It was observed that during the initial stage of growth ($t<0.1$ nm) the surface structure of the substrate is preserved, with the same RHEED pattern typical for a fourfold surface reconstruction (Fig. 1, second from top). After deposition of only 0.32 nm of $FeSn_2$, the fourfold surface reconstruction transforms into a fundamental diffuse pattern (Fig. 1, third from top), followed in short time ($t>\sim0.6$ nm) by a twofold surface reconstruction (Fig. 1, bottom). The latter is retained up to the final stages of growth of the $FeSn_2$ thin films. Further, it was observed that the initially long streaks transform into spots for thicknesses higher than 2 monolayers (ML), demonstrating three-dimensional (3D) growth of $FeSn_2$ islands.

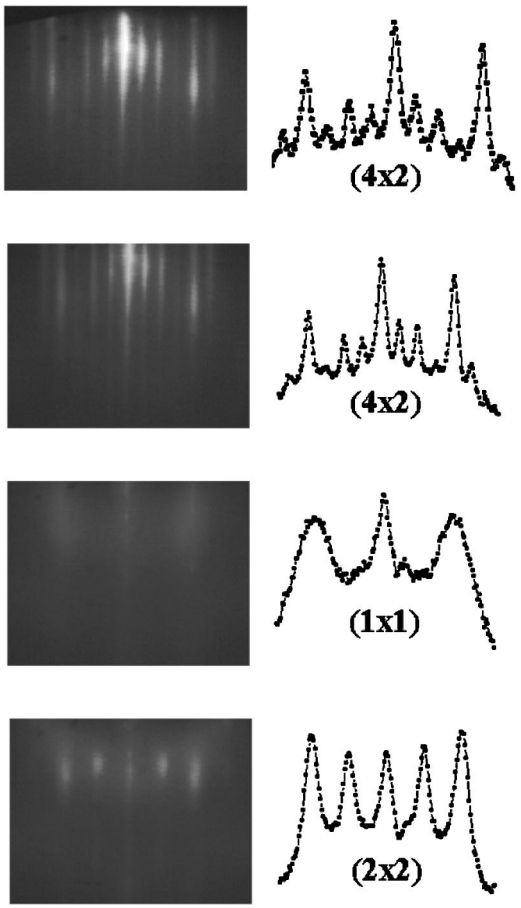

FIG. 1. Typical RHEED patterns (along the [110] azimuthal direction of InSb) of $FeSn_2(001)$ thin films grown at 250 °C on InSb(001). The images correspond to the following film thicknesses: clean InSb(001) surface (top), 0.10 nm (second from top), 0.32 nm (third from top), and 0.66 nm (bottom). Right-hand side: corresponding transversal intensity profiles. Electron energy: 10 keV.

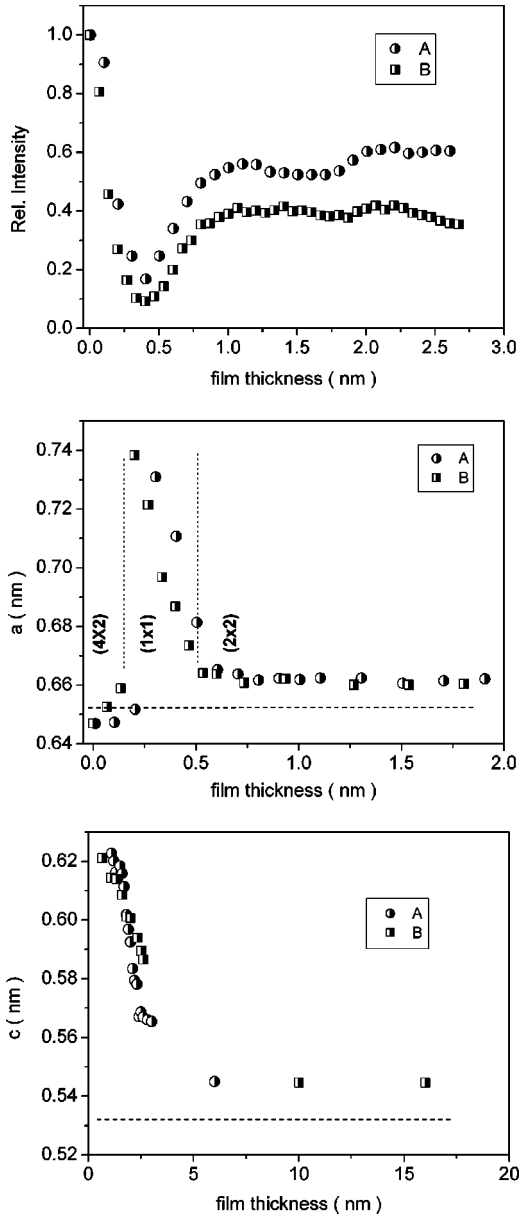

FIG. 2. (a) RHEED intensity of the (0,0) specular reflection during the growth at 250 °C of two $FeSn_2(001)$ thin films (samples A and B respectively). (b) In-plane lattice parameter of $FeSn_2(001)$ thin films (samples A and B, respectively) as a function of coverage. The value of 0.647 nm for bulk InSb was considered as the reference substrate lattice parameter. The horizontal dotted line corresponds to the lattice parameter *a* of the bulk $FeSn_2$ phase. (c) Out-of-plane lattice parameter of $FeSn_2(001)$ thin films as a function of coverage. A value of 0.647 nm for bulk InSb was considered as the reference substrate lattice parameter. The horizontal dotted line corresponds to the lattice parameter *c* of the bulk $FeSn_2$ phase.

This aspect is also observed in the evolution of the (specular) RHEED intensity of the (0,0) streak [Fig. 2(a)] measured in detail on two different samples (samples A and B). Samples A and B were prepared under similar conditions at a growth temperature of about 250 °C in order to demonstrate the reproducibility of growth and structure by RHEED. After reaching a pronounced minimum at a thickness of about 1 ML for both samples, the RHEED intensity [Fig. 2(a)] shows only weak oscillations, indicating the absence of perfect layer-by-layer growth, but rather 3D island growth. (The shift between the specular intensities of both samples [Fig. 2(a)] might be caused either by a difference in film roughness and/or by a small misadjustment of the angle of incidence of the RHEED beam). Accordingly, the spotty RHEED patterns obtained for films thicker than about 1 nm show intensity profile maxima along both the horizontal and vertical directions in the *k*-space. A typical RHEED pattern with its horizontal intensity profile is shown in Fig. 1 (bottom), and a RHEED pattern with its vertical intensity profile along the (0,0) streak is presented in Fig. 3. Under these conditions, both the in-plane and out-of-plane lattice parameters (*a* and *c*, respectively) of the $FeSn_2$ films relative to the InSb substrate lattice parameter may be calculated. The simple relationship derived from the Bragg formula, $d_f = (k_s/k_f)d_s$, with d_f and d_s the interplanar distances for film and substrate, respectively, and k_f and k_s the positions in *k*-space of the first-order diffraction spots relative to the zero-order reflection for film and substrate, respectively, was used. k_f and k_s were measured via the intensity profiles in pixels. The evolution of the measured *a* and *c* lattice parameters of samples A and B versus the film thickness is presented in Figs. 2(b) and 2(c), respectively. The reproducibility is good. A lattice parameter of 0.647 nm was assumed for

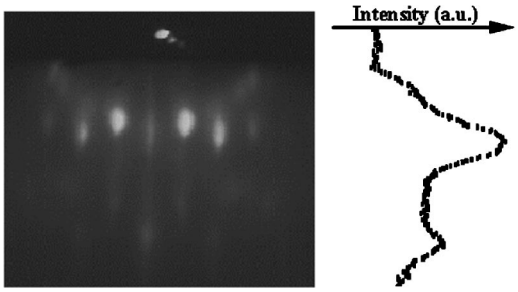

FIG. 3. RHEED pattern (along the [110] azimuthal direction of InSb) of a 2-nm-thick $FeSn_2$(001) film (sample B). Right-hand side: corresponding vertical intensity profile along the (0,0) spotty streak.

the InSb substrate. It is observed that the in-plane lattice parameter a of the film increases by 10% relative to that of InSb in the (1×1) reconstruction regime, and subsequently, in the usual (2×2) reconstruction regime, decreases to a constant value that is ~1% higher than the value of the bulk $FeSn_2$ compound. The out-of-plane lattice parameter [Fig. 2(c)] could be obtained only in the (2×2) reconstruction regime, where 3D growth occurs; c decreases strongly with the coverage from a value of about 0.620 nm (close to the InSb lattice constant) to a constant value of about 0.54 nm, which is 2% higher than the c value of the bulk $FeSn_2$ compound. The RHEED images obtained at $T_s=200\,^{\circ}\mathrm{C}$ were qualitatively similar to those at $T_s=250\,^{\circ}\mathrm{C}$ under otherwise similar conditions.

Within the elementary cell of $FeSn_2$, the Fe atoms occupy the $4a$ $(0,\ 0,\ \frac{1}{4})$ sites and the Sn atoms the $8h$ $(x,\frac{1}{2}+x,0)$ sites. A value of about 0.16 is reported[17] for the reduced coordinate, x. A top view (along the c axis) of the unit cell is sketched in Fig. 4. The LEED image at 54 eV obtained at 150 K on a 30-nm-thick (as-grown) $FeSn_2$ film (sample D) is presented in the middle of Fig. 4. The LEED pattern is schematically illustrated in Fig. 4. It is concluded from the LEED pattern that in reciprocal space the Fe reflections appear at a smaller distance from the symmetry center as compared to the Sn reflections, as expected from the atomic positions in real space. However, the angular separation of the pair of Sn reflections in reciprocal space appears to be lower than in the ideal compound. Indeed, by elementary geometrical considerations an x value of only 0.12(1) was deduced from the LEED pattern for the reduced coordinate, instead of 0.16, as reported for the bulk $FeSn_2$ compound.

The θ–2θ x-ray diffraction (XRD) diagrams of the as-grown $FeSn_2$ films indicate a high crystallographic texture along the c axis (perpendicular to the (001) film plane). Figure 5 exhibits the diffraction patterns of the InSb(001) substrate and of two epitaxial $^{57}FeSn_2/FeSn_2$ thin films (samples C and D, respectively) both grown at $T_s=200\,^{\circ}\mathrm{C}$, but with different thicknesses (Table I). The Miller indices of the most prominent peak are indicated in the same figure. At this point, it is worth mentioning that the two molecular beams ($FeSn_2$ is obtained by co-evaporation of Fe and Sn from two independent evaporation sources) are not perfectly parallel, and the two deposited areas on the substrate are not completely congruent. Consequently, the deposited thin films contain, except in the completely overlapping area, also a

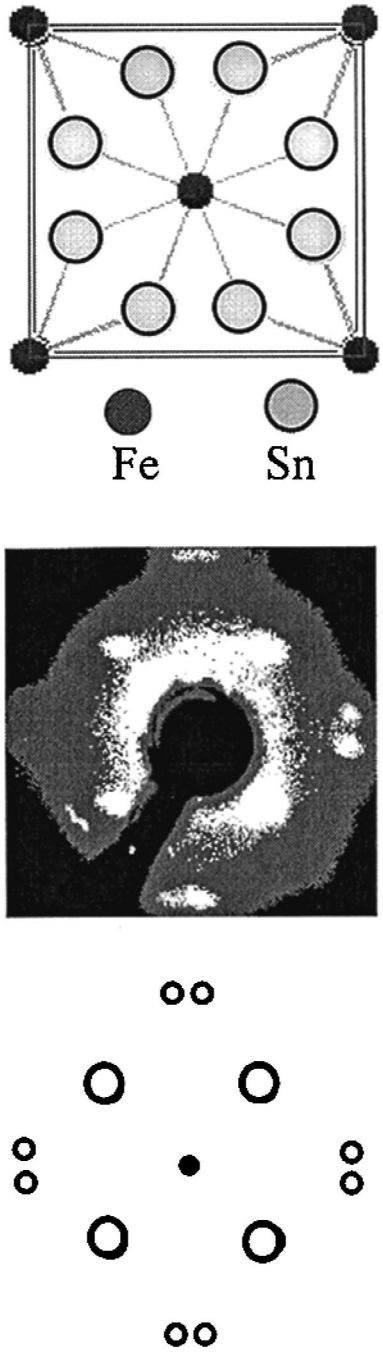

FIG. 4. Top view onto the (001) plane of the $FeSn_2$ unit cell (top). Middle: LEED pattern taken at 54 eV and at 150 K on a 30-nm-thick sample grown at 200 °C, (sample D). Bottom: schematics of the LEED pattern.

small outer area of pure Sn and bcc Fe, respectively. It is known that Sn grows on the InSb(001) substrate as epitaxial α-Sn(001) (cubic, $a=0.649$ nm),[21,22] whereas the Sn cap layer is expected to consist of polycrystalline β-Sn (tetragonal, $a=0.583$ nm, $c=0.318$ nm). The polycrystalline metallic Fe should give a negligible contribution to the diffraction pattern due to the cumulative effect of both, the very small area and randomly oriented reflection planes. Indeed, bcc Fe reflections have not been detected.

As observed in Fig. 5, the strong diffraction peaks at about 57° and 27° correspond to the reflection of the InSb(400) and (200) planes. For the thin film of 100-nm

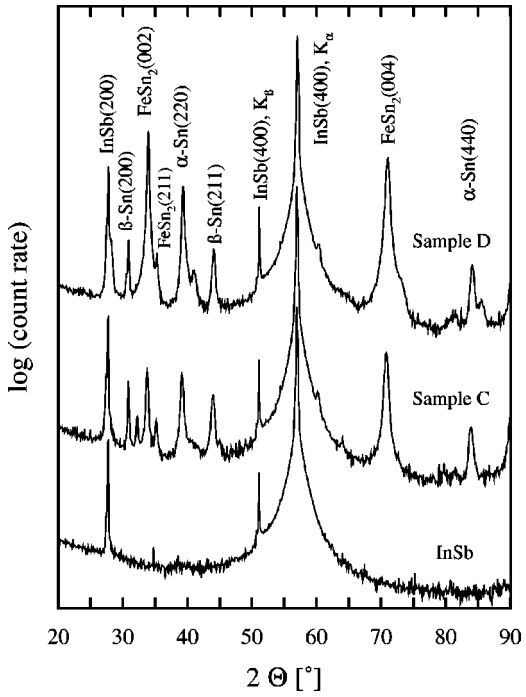

FIG. 5. Typical θ–2θ XRD patterns for two $FeSn_2$ thin films of different thicknesses ($t=100$ nm for sample C and $t=30$ nm for sample D), both grown at 200 °C on InSb(001). The diffraction pattern of the clean InSb(001) wafer is shown as a reference. The Miller indices of the most prominent peaks are presented as bar diagrams (Cu K_α radiation).

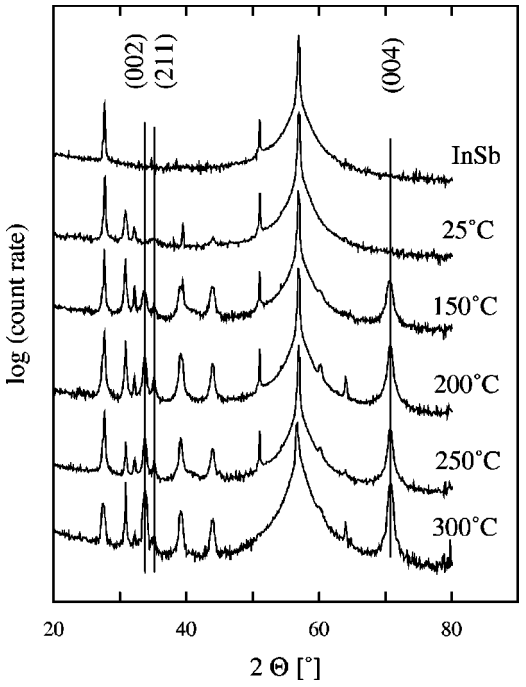

FIG. 6. θ–2θ XRD patterns of $FeSn_2$ thin films grown at different substrate temperatures on InSb(001), for clean InSb(001), and samples E(polycr.), H, D, G, and I (from top to bottom, respectively) (Cu K_α radiation).

thickness (sample C), additional strong diffraction peaks at about 34° [corresponding to the $FeSn_2$(002) reflection] and 70° [corresponding to the $FeSn_2$(004) reflection] as well as at about 39° [corresponding to the α-Sn(220) reflection] are observed in Fig. 5. The less pronounced peaks at about 30° and 44° belong to the β-Sn phase, and the weak peak at 35° to the (211) reflection of $FeSn_2$. For the thinner sample D ($t=30$ nm), the same Bragg peaks are detected; however, the intensity of the α- and β-Sn reflections now becomes comparable to the intensity of the $FeSn_2$ reflections. Special attention should be paid to the (002) and (211) peaks at 34° and 35°, respectively, belonging to the $FeSn_2$ phase, because there is no other additional phase producing an XRD signal in this angular interval. In a polycrystalline $FeSn_2$ phase with a reduced coordinate x in the unit cell that ranges from 0.12 to 0.16, the intensity of the (002) peak is about seven times lower than the intensity of the (211) peak. In a perfectly epitaxial (001)-oriented film, the (211) peak should give zero intensity. Therefore, the intensity ratio, $R=I_{002}/I_{211}$, gives valuable information about the degree of texture in the film along the film normal direction. This ratio has to increase drastically from a minimum value of $1/7\approx0.14$ for a fully polycrystalline thin film to a very high value, corresponding to a sharply textured films. In the present case, the observed values of $R>5$ correspond to a ratio N_{002}/N_{211} of the amount N_{002} of favorably oriented (002) planes (parallel to the sample surface) to the amount N_{211} of randomly oriented (002) planes of $N_{002}/N_{211}>5/0.14=36$. In other words, $[N_{002}-N_{211}]/N_{002}>0.97$, or more than 97% of the (002) planes are favorably oriented. Obviously there is a high degree of more than 97% of texture with the c axes perpendicular to the film surface. [In the case of $R>10$ (see later), the degree of texture is higher than 98.6%.] In this respect, the texture effects in different samples will be analyzed mainly via the evolution of the two peak intensities at 34° and 35°.

XRD patterns of various films [samples E(polycr.), H, D, G, and I] with thicknesses t between 15 and 30 nm and grown at different substrate temperatures are shown in Fig. 6. A weak and broad (211) diffraction peak at $2\theta\approx35°$ is present for the sample grown at 25 °C (sample E), providing evidence for a mainly polycrystalline $FeSn_2$ phase. For a substrate temperature of 150 °C, the (002) peak at 34° becomes already more pronounced than the (211) peak at 35°, but a certain amount of polycrystalline phase is still present. Taking into account the logarithmic intensity scale in Fig. 6, films grown at temperatures higher than 200 °C show very strong structural texture of more than 98.6% with the c axis along the film normal direction ($R>10$), proving (together with the RHEED and LEED patterns) that good epitaxial growth of the $FeSn_2$ phase is achieved. It is worth mentioning that the RHEED pattern of sample E ($T_s=25$ °C, $t=15$ nm) has shown, instead of the dotty streaks, smooth Debye–Scherrer diffraction rings, typical for polycrystalline samples.

2. Mössbauer investigations

Mössbauer (CEMS) spectra of the as-grown sample D ($T_s=200$ °C, $t=30$ nm), taken at different temperatures, are presented in Fig. 7. The sextets have been fitted with a distribution of hyperfine fields, $P(B_{hf})$. At 80 K, the spectrum consists of a Zeeman-split magnetic sextet with a measured peak hyperfine field B_{hf} of 15.0(1) T and an isomer shift

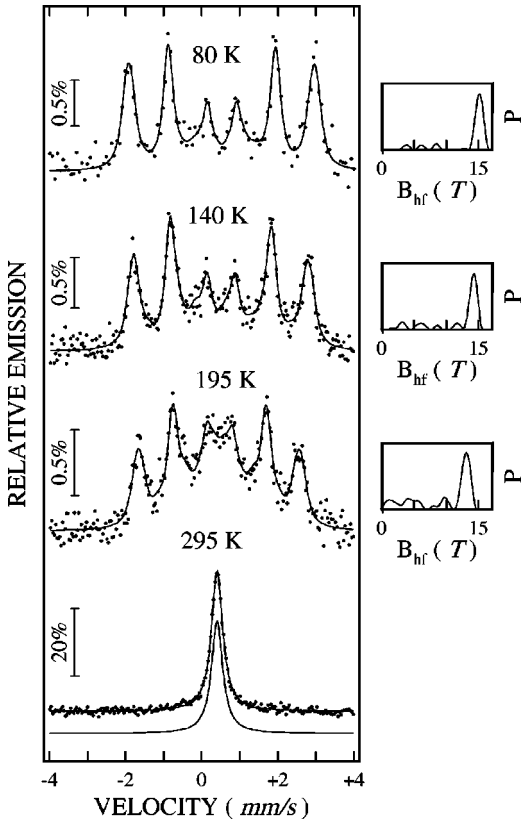

FIG. 7. Mössbauer (CEMS) spectra of sample D "as-grown" ($T_s = 200\,^{\circ}\mathrm{C}, t = 30$ nm) taken at different temperatures. Right-hand side: corresponding hyperfine field distributions, $P(B_{\mathrm{hf}})$.

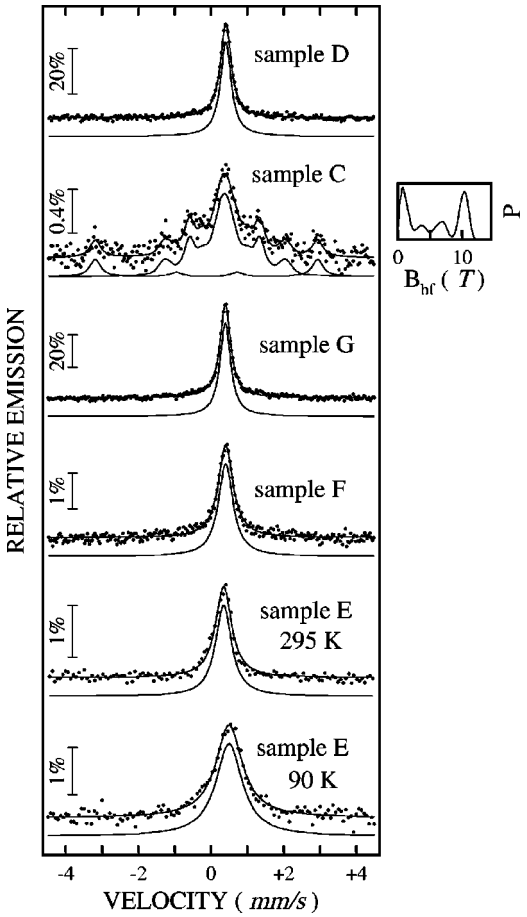

FIG. 8. RT Mössbauer spectra and corresponding hyperfine field distributions for "as-grown" samples with different thicknesses t (from top to bottom): sample D ($t = 30$ nm, $T_s = 200\,^{\circ}\mathrm{C}$), sample C ($t = 100$ nm, $T_s = 200\,^{\circ}\mathrm{C}$), sample G ($t = 15$ nm, $T_s = 250\,^{\circ}\mathrm{C}$), sample F ($t = 30$ nm, $T_s = 250\,^{\circ}\mathrm{C}$), and sample E (polycr.) ($t = 15$ nm, $T_s = 25\,^{\circ}\mathrm{C}$). Bottom: sample E (polycr.) measured at 90 K.

(relative to bcc Fe at RT) of about +0.5 mm/s, in agreement with the spectral parameters of the AF $FeSn_2$ phase at low temperature, reported earlier.[15,16] By increasing the measurement temperature, the magnitude of B_{hf} decreases rapidly, and the spectrum of sample D at RT collapses to a paramagnetic singlet (isomer shift +0.40(1) mm/s, linewidth 0.35(1) mm/s). A Néel temperature of about 250(10) K may be estimated from the temperature dependence of the hyperfine field of sample D. The relatively low Néel temperature of this film may be related to either a finite thickness effect and/or to structural effects, such as deviations from stoichiometry and from perfect chemical ordering, indicating Fe and Sn atomic site disorder.

Additional Mössbauer experiments on epitaxial $FeSn_2$ films grown under similar conditions, but with different thicknesses, were performed in order to elucidate this aspect. This concerns in particular the pair of samples C, D. The RT Mössbauer spectra taken on samples D ($T_s = 200\,^{\circ}\mathrm{C}, t = 30$ nm), C ($T_s = 200\,^{\circ}\mathrm{C}, t = 100$ nm), G ($T_s = 250\,^{\circ}\mathrm{C}, t = 15$ nm), F ($T_s = 250\,^{\circ}\mathrm{C}, t = 30$ nm), and E(polycr.) ($T_s = 25\,^{\circ}\mathrm{C}, t = 15$ nm) are shown in Fig. 8. The thicker film (sample C) shows a spectrum in the transition region from antiferromagnetism to paramagnetism, whereas for the thinner samples D, F, G, and E(polycr.), the magnetic patterns are collapsed to a single line, with a narrower linewidth for the thinnest film (sample G). The spectral parameters of the singlets at RT are as follows: (i) isomer shift +0.40(1) mm/s (sample F), +0.38(1) mm/s (sample G), and +0.34(1) mm/s [sample E(polycr.)]; (ii) linewidth 0.46(1) mm/s (sample F), 0.36(1) mm/s (sample G), and 0.52(1) mm/s [sample E(polycr.)]. Additional traces of bcc Fe as an artifact are evident in the Mössbauer spectrum of sample C (Fig. 8), arising as an artifact from the nonoverlapping outer area of the co-evaporated molecular beams on the substrate (iron part). A Néel temperature above RT is evident for sample C, and T_N values lower than RT result for samples D, F, G, and E(polycr.). Accordingly, considering the influence of the film thickness at the same growth temperature, sample C ($T_s = 200\,^{\circ}\mathrm{C}, t = 100$ nm) with the larger thickness exhibits a higher Néel temperature than the thinner sample D ($T_s = 200\,^{\circ}\mathrm{C}, t = 30$ nm). Apparently, T_N increases with the total $^{57}FeSn_2/FeSn_2$ layer thickness t. From the larger linewidth of 0.88(1) mm/s at 90 K as compared to 0.52(1) mm/s at 295 K (RT), a low Néel temperature around 90 K is estimated for 15-nm-thick polycrystalline $^{57}FeSn_2/FeSn_2$ (sample E) grown at a 25 °C.

Generally, a reduction of the magnetic ordering temperature (relative to its bulk value) with decreasing film thickness (finite size effect) is expected from theoretical considerations.[23] In fact, a drastic finite size effect below 100 nm thickness was reported for metallic spin-glass thin

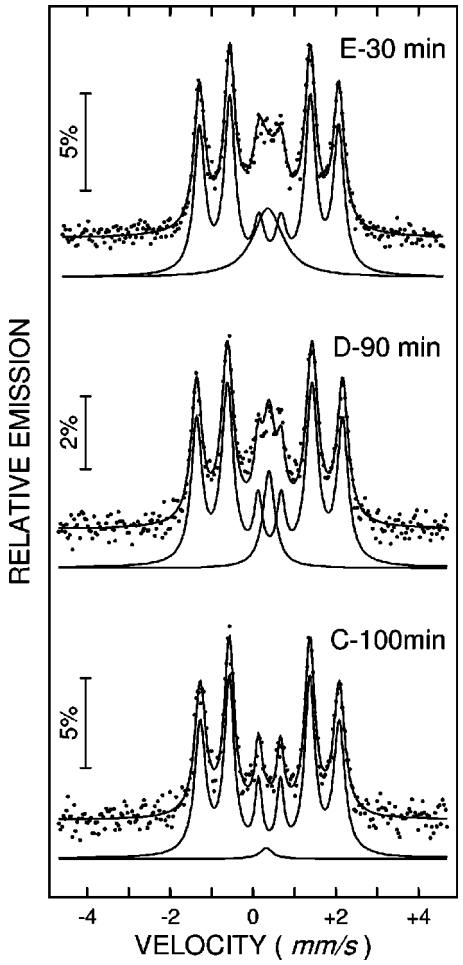

FIG. 9. RT Mössbauer spectra of samples E ($T_s = 25\,°C, t = 15$ nm), D ($T_s = 200\,°C, t = 30$ nm), and C ($T_s = 200\,°C, t = 100$ nm) after isothermal annealing at a temperature of 350 °C for different annealing times (30, 90, and 100 min, respectively).

films,[24] which are characterized by competing long-range FM and AF interactions. Since $FeSn_2$ is also metallic system (possibly with long-range AF interactions), our observation of a T_N reduction with decreasing film thickness is not surprising.

The line intensity ratio of the $^{57}FeSn_2$-Zeeman sextet was found to be 3:4:1:1:4:3 from the least-squares fitting of the spectra in Figs. 7 and 8. This demonstrates that the Fe spins in the 5- to 15-nm-thick $^{57}FeSn_2$ top layers of the different samples are oriented in the (001) film plane, as expected from the compensated AF Fe spin structure of the bulk $FeSn_2(001)$ surface.

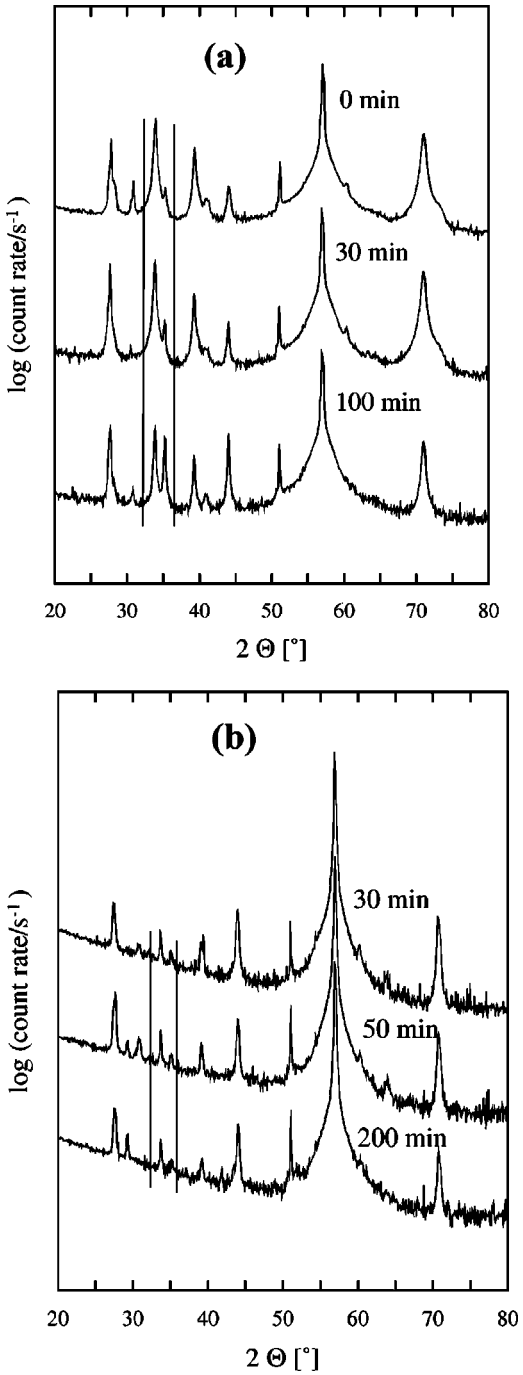

FIG. 10. (a) XRD patterns of sample C ($T_s = 200\,°C, t = 100$ nm) after isothermal annealing at a temperature of 350 °C for different annealing times. (b) XRD patterns of sample F ($T_s = 250\,°C, t = 30$ nm) after isothermal annealing at 300 °C for different annealing times. The (002) and (211) reflections lie between the two dotted vertical lines.

B. Films after thermal annealing

Since in exchange-bias bilayer systems, AF thin films with thicknesses of tenths of nanometers and Néel temperatures higher than RT are of interest, we considered the possibility of increasing T_N of the epitaxial $FeSn_2(001)$ thin films by suitable thermal annealing. RT Mössbauer spectra of samples E, D, and C after isothermal annealing at 350 °C under UHV conditions for different annealing times are presented in Fig. 9. They consist of a dominant magnetic sextet superimposed to a less intense paramagnetic central singlet. The magnetic sextet with a hyperfine field of 10.5(1) T, an isomer shift of +0.40(1) mm/s, and a line intensity ratio of 3:4:1:1:4:3 indicates the presence of a ordered stoichiometric $FeSn_2$ phase with a Néel temperature well above RT and in-plane oriented Fe spins. However, the degree of atomic disorder between the Fe and Sn sites appears to be not completely removed by the thermal treatments, because the weak paramagnetic (central) singlet component in the Mössbauer spectra, with an isomer shift of +0.34(2) mm/s and a line-

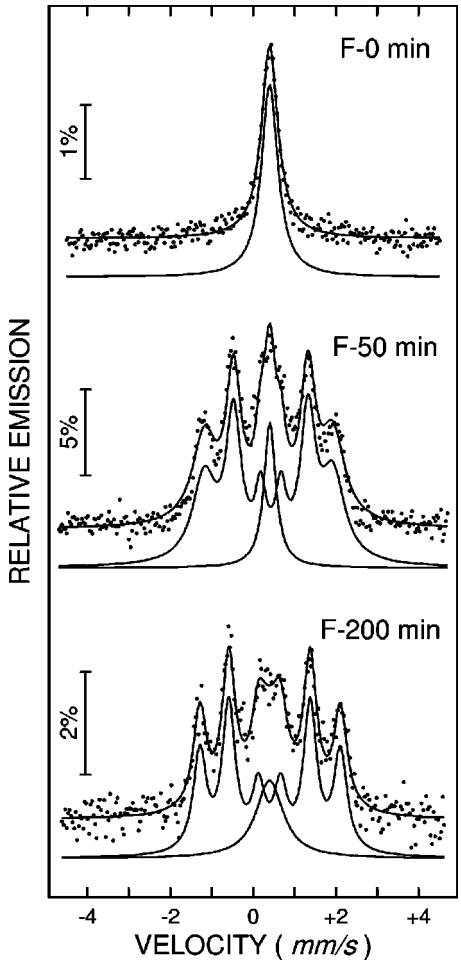

FIG. 11. Mössbauer spectra of sample F ($T_s = 250\,^{\circ}\mathrm{C}, t = 30$ nm) after isothermal annealing at a temperature of 300 °C for different annealing times.

width ranging from 0.50 mm/s (sample D) to 0.80 mm/s [sample E(polycr.)], is still observed. The singlet presumably originates from Fe atoms in the rest of the chemically disordered volume fraction. The higher the relative spectral area of the magnetic sextet in the Mössbauer spectrum, the higher the degree of the correct atomic occupation at the Fe and Sn sites. Both the final stage of the degree of atomic ordering and the dynamics of the ordering process, are dependent on the film thickness, the annealing temperature and the annealing time. For an annealing temperature of 350 °C atomic ordering is almost completely achieved in sample C (more than 98% relative spectral area of the magnetic sextet) after a treatment of 100 min (Fig. 9). Unfortunately, for such a temperature, the degree of crystallographic texture along the *c* axis decreases with the annealing time (the XRD ratio $R = I_{002}/I_{211}$ decreases to about 1 for treatments longer than 100 min), as can be seen in the XRD patterns of Fig. 10(a). Annealing treatments at lower temperatures (e.g., 300 °C) preserve the degree of *c*-axis texture over a long annealing time [Fig. 10(b)], but according to the CEM spectra of sample F in Fig. 11, the degree of atomic disorder remains at a relatively high level (about 18% in relative spectral area for the paramagnetic singlet after 200-min annealing, Fig. 11, bottom).

IV. CONCLUSION

$^{57}FeSn_2/FeSn_2(001)$ thin films with total thicknesses ranging from 15 to 100 nm and covered by a 5-nm-thick Sn cap layer have been epitaxially grown on clean InSb(001) substrates by MBE. Tracer layers of $^{57}FeSn_2(001)$ 5- to 15-nm-thick on top of the natural $FeSn_2(001)$ films were usually included in order to perform ^{57}Fe CEMS measurements. Different substrate temperatures were used during the deposition process.

The film epitaxy was studied by *in situ* RHEED and LEED, and *ex situ* XRD. Good epitaxial films were obtained for growth temperatures higher than 150 °C and lower than 300 °C, for all the considered thicknesses. The in-plane lattice parameter [relative to that of the InSb(001) substrate] of the $FeSn_2(001)$ overlayer as a function of coverage increases initially by 10% and subsequently decreases and saturates at an only 2% higher value. The out-of-plane lattice parameter of the film *c* decreases continuously from an initial value close to that of InSn to a value approaching the *c* value of the bulk $FeSn_2$ phase. A value of 0.12 was deduced from the LEED patterns for the reduced atomic coordinate *x* in the $FeSn_2$ unit cell.

The relatively low Néel temperature found for the as-grown epitaxial films is presumably due mainly to the atomic site disorder, but finite thickness effects are also involved. The correct occupation of the proper atomic sites can be improved by suitable annealing treatments. The optimal activation energy for such a process corresponds to a temperature between 300 and 350 °C. Higher temperatures destroy the epitaxy, whereas lower temperatures are not efficient in promoting $FeSn_2$-type atomic ordering. The Fe atomic magnetic moments are found to be oriented in the plane of the Sn-coated $FeSn_2(001)$ films. We conclude that epitaxial $FeSn_2(001)$ thin films with T_N above room temperature are suitable antiferromagnets for investigating the interfacial spin structure in exchange-biased FM/$FeSn_2$ bilayers by ^{57}Fe CEMS.

ACKNOWLEDGMENTS

The valuable technical assistance by U. v. Hörsten is gratefully appreciated. This work was sponsored by the Deutsche Forschungsgemeinschaft (SFB 491). Financial support through the Alexander-von-Humboldt-Stiftung is gratefully acknowledged (V. K.).

[1] J. Fujikata, K. Hayashi, H. Yamamoto, and K. Yamada, J. Magn. Soc. Jpn. **19**, 365 (1995).
[2] J. C. S. Kools, IEEE Trans. Magn. **32**, 3165 (1996).
[3] B. Dieny, V. S. Speriosu, S. S. P. Parkin, B. A. Gurney, D. R. Wilhoit, and D. Mauri, Phys. Rev. B **43**, 1297 (1991).
[4] B. Dieny, J. Magn. Magn. Mater. **136**, 335 (1994).
[5] W. H. Meiklejohn and C. P. Bean, Phys. Rev. **102**, 1413 (1956).
[6] D. Mauri, H. C. Siegmann, P. S. Bagus, and E. Kay, J. Appl. Phys. **62**, 3047 (1987).
[7] A. P. Malozemoff, J. Appl. Phys. **63**, 3874 (1988).
[8] N. C. Koon, Phys. Rev. Lett. **78**, 4865 (1997).
[9] T. C. Schulthess and W. H. Butler, Phys. Rev. Lett. **81**, 4516 (1998); J. Appl. Phys. **85**, 5510 (1999).

[10] U. Nowak, A. Misra, and K. D. Usadel, J. Appl. Phys. **89**, 7269 (2001).
[11] Ch. Sauer and W. Zinn, in *Magnetic Multilayers*, edited by L. H. Bennett and R. E. Watson (World Scientific, Singapore, 1993).
[12] M. Przybylski, Hyperfine Interact. **113**, 135 (1998).
[13] T. Shinjo and W. Keune, J. Magn. Magn. Mater. **200**, 598 (1999).
[14] W. Keune, V. E. Kuncser, M. Doi, M. Askin, H. Spies, B. Sahoo, E. Dunman, M. Acet, J. S. Jiang, and S. D. Bader, J. Phys. D **35**, 2352 (2002).
[15] V. I. Nikolaev, Yu. I. Shcherbina, and Karchevskii, JETP **44**, 775 (1963); JETP **17**, 524 (1963).
[16] V. I. Nikolaev, Yu. I. Shcherbina, and S. S. Yakimov, JETP **45**, 1277 (1963).
[17] G. LeCäer, B. Malaman, G. Venturini, D. Fruchart, and B. Roques, J. Phys. F: Met. Phys. **15**, 1813 (1985).
[18] G. Venturini, D. Fruchart, J. Hübsch, G. LeCaer, B. Malaman, and B. Roques, J. Phys. F: Met. Phys. **15**, 427 (1985).
[19] V. Kuncser, F. Stromberg, B. Sahoo, W. Keune, E. Duman, and M. Acet (unpublished).
[20] R. A. Brand, Nucl. Instrum. Methods Phys. Res. B **28**, 398 (1987); the NORMOS program is available from Wissel GmbH, D-82319 Starnberg, Germany.
[21] H. Omi, H. Saito, and T. Osaka, Phys. Rev. Lett. **72**, 2596 (1994).
[22] B. Roldan Cuenya, M. Doi, O. Marks, W. Keune, and K. Mibu, in *Structure and Dynamics of Heterogeneous Systems*, edited by P. Entel and D. E. Wolf (World Scientific, Singapore, 2000), p. 2.
[23] M. E. Fisher, J. Vac. Sci. Technol. **10**, 665 (1973).
[24] J. A. Cowen, G. G. Kenning, and J. Bass, J. Appl. Phys. **64**, 5781 (1988).